Freeform Fabrication of Ti$_3$SiC$_2$ Structures

D.J. Dcosta and W. Sun[1]
Department of Mechanical Engineering and Mechanics

T. EI-Raghy
Department of Materials Engineering

Drexel University
Philadelphia, PA 19104

This paper introduces a three-stage process to fabricate highly dense Ti$_3$SiC$_2$ structures. The properties of Ti$_3$SiC$_2$ material, the synthesis of the ceramic powder, the procedure involved in the 3-stage fabrication process and the preliminary results on fabricating fully dense Ti$_3$SiC$_2$ structures are presented. The characterization and microstructure evaluation of the mechanical, morphological and structural properties covering the compressive strength, Vickers micro hardness, damage tolerance, thermal shock, shrinkage and porosity of Ti$_3$SiC$_2$ structures printed using the 3-stage process are presented.

1. Introduction

Quite a few researches have used freeform fabrication techniques to directly prototype functional ceramic parts in order to obtain more freedom in the design and utilization of ceramic structures [1]. Studies include photopolymer resin curing by ultraviolet light employing SLA and solid ground curing [2], thermal fusion of powders by laser scanning used in the SLS process [3], adhesion of powders by disbursal of binder through an ink-jet used in three-dimensional printing [4-6], compacting and sintering of powders as demonstrated in the freeform powder molding technique [7], extrusion of thermoplastics through a fixed diameter nozzle in the FDM process [8], using an extension of the 3D Printing technique to build objects of variable density by controlling microstructure and composition [9], and Multiphase Jet Solidification (MJS) [10]. Another technique involved a further development to the technology of Inkjet Printing, wherein, the binder in the printing cartridge was replaced by a ceramic suspension, pressurized in a continuous ink jet printer [11,12]. Similar techniques such as Robocasting [13], involving a computer-aided deposition of highly concentrated ceramic colloidal slurries directly forming complex shapes without the use of molds or dies have also been researched upon. Additionally, other similar techniques relying on the basic inkjet printing technology are the overprinting technique [14] using inkjet printing of electro ceramics such as lead zirconate titanate (using a piezoelectric actuator to eject the ink); electro photographic powder deposition [15] technique employing the deposition of charged powder particles layer-by-layer, resulting in the precise deposition of particles to the desired shape; electromagnetic ink jet printing [16] employing the ejection of ceramic inks via an electromagnetic valve printing head and dispersion of ceramic inks onto a substrate using an ultrasonic vibrating horn have also been experimented upon.

---

[1] Corresponding author, Tel: 215-895-5810; Fax: 215-895-2094; Email: sunwei@drexel.edu

The objective of this paper is to present our preliminary studies on using Layered Printing, compacting, and sintering processes to fabricate fully dense functional Titanium Silicon Carbide (Ti_3SiC_2) structures with the comparable properties to the Ti_3SiC_2 bulk reported in [17-20]. The contents of this paper are presented as follows. Section 2 briefly reviews the properties of Ti_3SiC_2 and the ceramic powder preparation. Section 3 describes the 3-stage process. The fabricated samples are presented in Section 4. The results of structural characterization, such as the compressive strength, Vickers micro hardness, damage tolerance, thermal shock, shrinkage and porosity and microstructure evaluation, of Ti_3SiC_2 structures are presented in Section 5. Summary, conclusion and discussions are presented in Section 6.

2. Ti_3SiC_2 - Properties and Powder Preparation

Titanium Silicon Carbide, a layered ternary ceramic compound was processed in bulk, by Dr. M. W. Barsoum and Dr. T. El-Raghy at Drexel University. Polycrystalline bulk samples of Ti_3SiC_2 were synthesized by reactively hot pressing Titanium, Graphite (Carbon) and Silicon Carbide powders at a pressure of 40 MPa and temperature of 1600 ^{o}C for 4 hours at a temperature rate of 10 ^{o}C/min. [18 - 20]. The bulk sample obtained as a result of the solid phase reaction was milled to obtain a ceramic powder. As a part of the powder preparation process pure Ti_3SiC_2 powder is thoroughly mixed with a water-soluble binder and dried to form clinker. The resulting clinker is crushed in a powder mill. As a result of this entire process fine Ti_3SiC_2 powder particles coated with a film of binder are obtained. Further, the powder was sifted through a –325 mesh sieve to obtain an average grain size of less than 40 μm. This batch of powder was used as the build powder in our study.

Ti_3SiC_2 possesses a unique combination of mechanical, electrical and thermal properties of both metals and ceramics. Like metals it is an excellent electrical and thermal conductor, easily machinable, relatively soft, good thermal shock resistance and behaves plastically at higher temperatures, and like ceramics it is oxidation resistant and refractory in nature[18,19]. It has an electrical conductivity of 4.5 x 10^6 ohm^{-1} m^{-1} that is twice that of pure Titanium (2.3 x 10^6 ohm^{-1} m^{-1}). The thermal expansion coefficient, in the temperature range of 25 to 1000 ^{o}C, the room temperature thermal conductivity and heat capacity are 9.2 x 10^{-6} ^{o}C-1, 43 W/m K and 588 J/kg K respectively, these being similar to that of Titanium namely, 31 W/m K and 523 J/Kg K. Its density of 4.5 gm/cc is roughly half the density but almost double the stiffness of Nitrogen based super-alloys. Ti_3SiC_2 is relatively soft with Vickers Hardness of 2-5 GPa but elastically stiff and easily machinable.

A remarkable property of Ti_3SiC_2 carbide is its easy machinablility in spite of its high stiffness. The layered structure of material and its ductility contributes to direct machinability to close tolerances without any post machining sintering, whereas in other cases the ceramic needs to be sintered after machining resulting in an additional shrinkage. Ti_3SiC_2 is the only carbide that can be cut manually using a hacksaw. Due to its good electrical properties it is also easily shaped and cut using Electric Discharge Machining. In addition, Ti_3SiC_2 retains its mechanical properties at high temperatures and is stable at temperatures of 1800 ^{o}C with excellent high temperature mechanical properties [20]. There is no effect on the bend strength of Ti_3SiC_2 when heated to 1400 ^{o}C and quenched. This ceramic actually increases in strength and exhibits excellent resistance to thermal shock, whereas other ceramics have a drastic reduction in strength

when subjected to the same conditions of quenching. The structural properties of samples developed using the 3-stage integrated process have been evaluated in Section 5.

3. The Three-Stage Fabrication Process

The fabrication of Ti_3SiC_2 structure is divided into three primary stages [21]: 1) solid freeform fabrication, 2) pressure compacting, and 3) Sintering. Flow chart of the 3-stage process is described in Figure 1. In the first stage, the part is built using the layered Printing technique employing the powder deposition and liquid binding technique to print the part as a layered structure, wherein the Ti_3SiC_2 powder is used as the build material. In this process the STL file generated from the corresponding CAD model is inputted to the prototyping system to generate the process path. The green part is built by deposition of Ti_3SiC_2 powder and binder spray (as per the cross-section at the particular slice) layer by layer till the entire part is built. At this stage the green part has been freshly developed and has a low structural strength. The second stage is to compact the green part by applying a high pressure on the green part to increase the density and the strength of the green part. The last stage of the process is to sinter the compacting part in an electric tube furnace at high temperature in a flowing Argon atmosphere (inert atmospheric conditions are specified to prevent any oxidation).
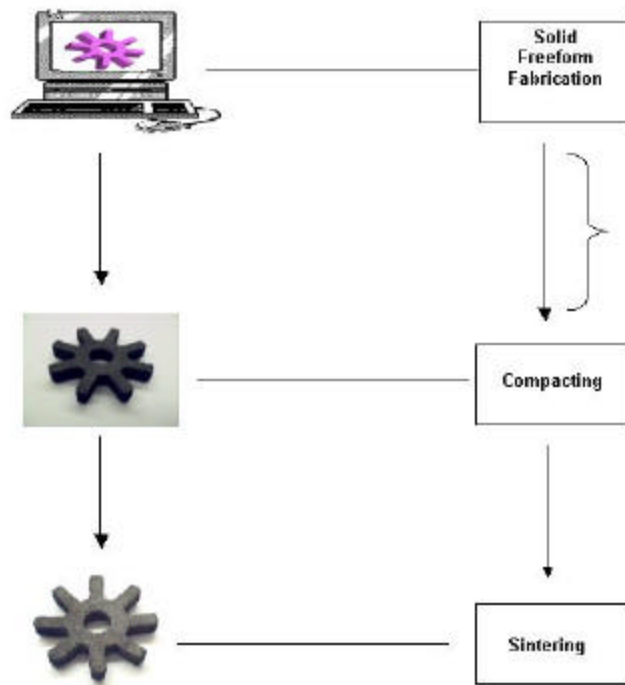

Figure 1: Three-stage fabrication process for Ti_3SiC_2 structures

4. Fabrication of Ti_3SiC_2 Samples

To understand the effect of the compacting pressure on the structural properties of the Ti_3SiC_2 samples, two sets of samples were processed. One set of samples was fabricated using the integrated 3-stage process, i.e., SFF, Compacting, and Sintering. While the other set was sintered directly without Compacting after SFFP. The samples without the compacting process

were fabricated with layer thickness of 0.0035", 0.007" and 0.01" and the binder concentration of 7 – 40%. Standard procedures were used to prepare samples for structural and optical characterization.

Figure 2 shows different Ti_3SiC_2 samples fabricated through the 3-stage process, such as a 6-tooth sprocket, turbine wheel and hollow tube (Figure 2), and the master sample for test and characterization (Figure 3). Figure 2a to 2c show the samples at different process stages, namely, SFF green parts (2a), compacted parts (2b), and sintered parts (2c). The master sample shown in Figure 3 was used as the test specimen. Test samples for mechanical property evaluation were derived from the master sample. The layer thickness for fabricating the master sample was fixed at 0.0035". The densities achieved for samples fabricated using the 3-stage technique were over 99%.
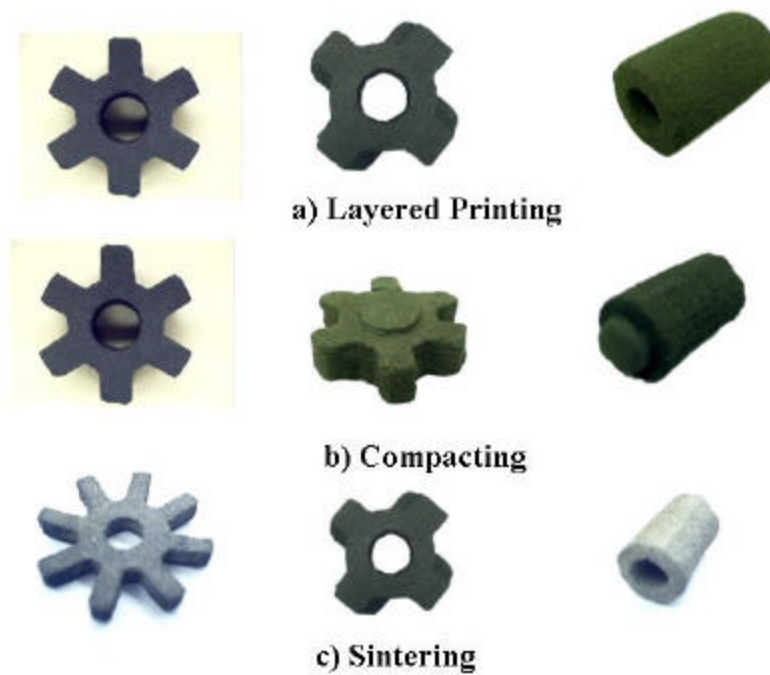

a) Layered Printing

b) Compacting

c) Sintering

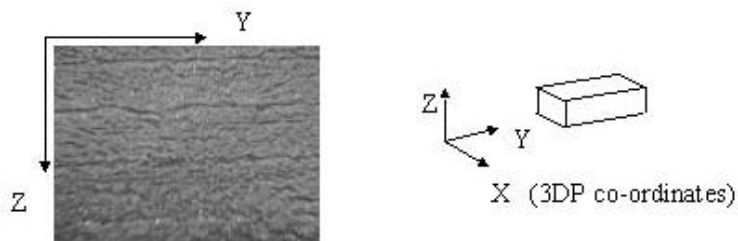Figure 2: Parts fabricated using the 3-stage process

Figure 3: Master sample (layered structure) fabricated using the 3-stage process

5. Mechanical Testing and Microscopic Evaluation

The mechanical testing and microscopic evaluation of the prototyped Ti_3SiC_2 samples were conducted to evaluate the compressive strength, Vickers micro hardness, damage tolerance, thermal shock, shrinkage and porosity (Figure 4). A summary of the results is presented in this section. Comparisons have been made with the available data reported in the references. It needs to be pointed out that the Ti_3SiC_2 powder batch used in our samples contained about 30 – 40% more TiC (Titanium Carbide) than the powder used in reference [20], and hence the results reported here are higher than the reported data due to the presence of the excessive amount TiC.
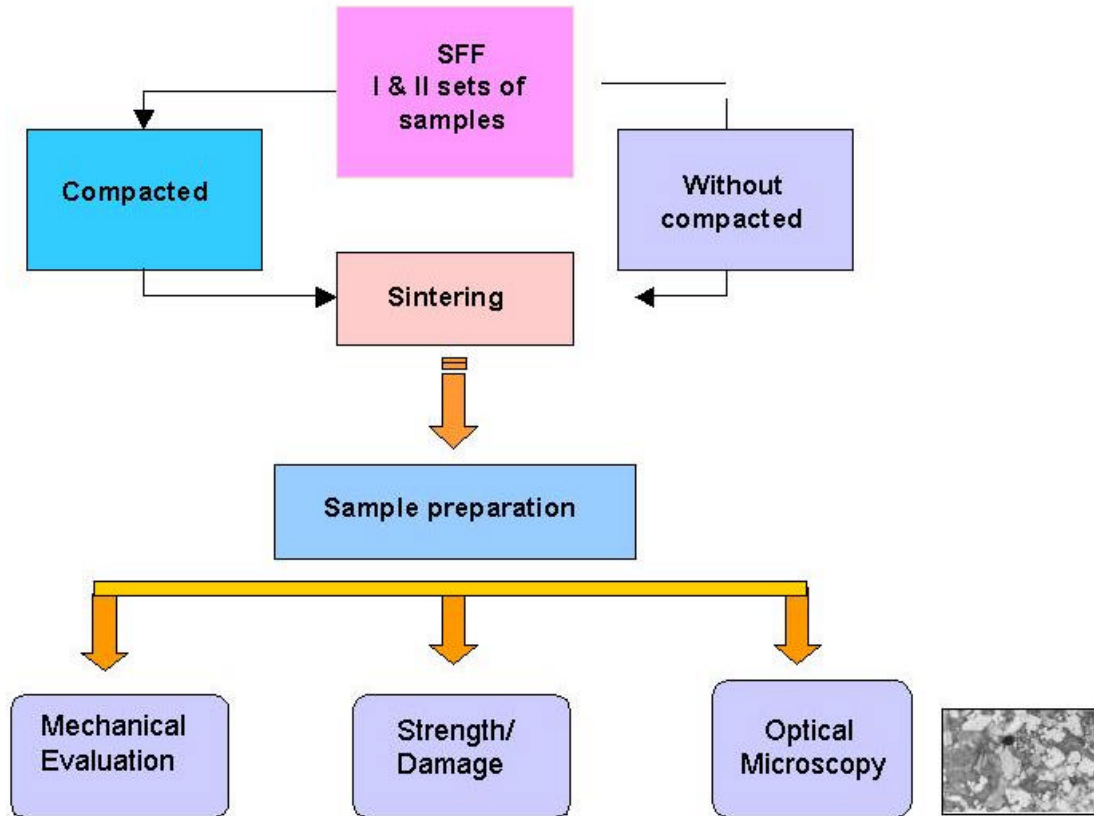

Figure 4: Mechanical characterization and microscopic evaluation of Ti_3SiC_2 test samples

The test specimens were cut from the master sample (Figure 3) using an EDM. Parallel machining was ensured to minimize any irregularities in dimensions of the test samples. For the evaluation of micro hardness and optical microstructure, samples cut from the master sample. were subjected to a grinding sequence of 300, 500 and 1200 grit Silicon Carbide paper and later polished to a mirror finish on 3 µm and 1 µm diamond suspension using a Struers Rotopol automatic polishing machine.The specimens for compression testing were cut from the master sample in the X and Z axes of the printing development, and for damage tolerance and thermal shock in the X and Y axes of the printing development. The sides of the specimen were ground on 800 and 1200 grit Silicon Carbide paper to remove burrs and flashes. This was done to minimize the possibility of error during the four point bend test. The specimens for the damage tolerance tests were marked with an indentation using a Vickers Indenter, on the tensile side of the specimen with indentation loads of 100, 200 and 300 N. It was ensured that the indentation

was in the region of maximum bending of the specimen. The samples for the thermal shock tests were heated upto pre-quench temperatures of 400 $^{\circ}$C, 800 $^{\circ}$C and 1200 $^{\circ}$C.

5.1 Compression Strength

The compression tests were conducted on test specimens measuring 3mm x 3mm x 6mm cut along the X and Z axes of the printing using a servo-hydraulic testing machine (MTS System, Eden Priarie, MN) at a constant crosshead speed of 0.01 mm/s. Friction and mutual sliding between the Testing Machine platens and the specimen surfaces was minimized by the application of anti-friction grease. The breaking stress in compression was calculated as:

$$s = Load / Area$$

The Load – Displacement curve is presented in Figure 5. It is observed that the deformation in compression of the test specimen is linear to failure and does not exhibit any plastic deformation behavior, with the failure being that of a brittle fracture. The results of the compression tests were calculated based on an average of five measurements. The average breaking strength in compression at a breaking load of 10.3 KN was found to be 1144.44 MPa in the XY plane of the printing, and at a breaking load of 11.03 KN was 1225 MPa in the Z plane, both at a strain rate of 0.0016/s. The observed difference in strength along the two independent planes or axes leads us to believe that the strength property is anisotropic due to the Layered Printing process. Although the micrographs (presented later) do not reveal any texture in the specimen, we believe that there is a process-induced anisotropy in the printed structure. The reported compressive strength of compacted and sintered (without SFF) coarse-grained Ti_3SiC_2 samples at room temperature is 720 MPa [20]. The test results conform to the reported compressive strength values for compacted (without SFF) and sintered coarse-grained Ti_3SiC_2 samples, with a proportional increase observed due to the presence of 30 – 40% of TiC.
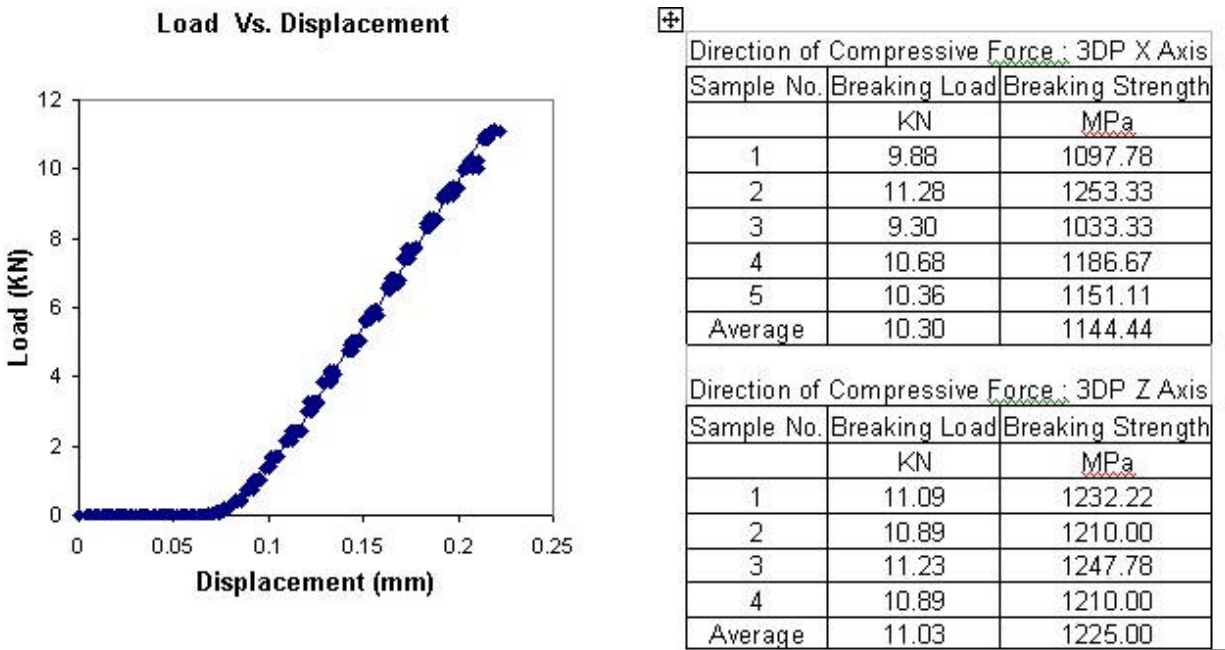
Load Vs. Displacement

Direction of Compressive Force : 3DP X Axis		
Sample No.	Breaking Load	Breaking Strength
	KN	MPa
1	9.88	1097.78
2	11.28	1253.33
3	9.30	1033.33
4	10.68	1186.67
5	10.36	1151.11
Average	10.30	1144.44

Direction of Compressive Force : 3DP Z Axis		
Sample No.	Breaking Load	Breaking Strength
	KN	MPa
1	11.09	1232.22
2	10.89	1210.00
3	11.23	1247.78
4	10.89	1210.00
Average	11.03	1225.00

Figure 5: Load - Displacement curve and compressive strength

208

5.2 Vickers Micro Hardness

The micro-hardness test was conducted on polished sample surfaces using a Leco M-400 (St. Joseph, MI) diamond indenter at loads of 1, 3, 5 and 10 N. The diagonal values of the indentations were measured, an average of the diagonal lengths (Figure 6) was calculated and a conversion was obtained from the corresponding Vickers charts to derive the Vickers Micro Hardness.

Micrograph   **Schematic**

Figure 6: Indentation obtained using Leco M400 Micro Hardness Tester

The micro hardness values have been presented as an average of five measurements. The hardness obtained for the samples was in the range of 12.3 – 9.4 GPa for an indentation load of 1 – 10 N (Figure 7). Further, the hardness seemed to have stabilized at 9 GPa, i.e, Vickers Hardness at increased loads will result in the stabilized value. The Vickers hardness of compacted and sintered (without SFF) Ti_3SiC_2 samples has been reported to be in the range of 8 - 4 GPa for samples obtained from fine grained Ti_3SiC_2 with load increasing from 1 N to 100 N, and for coarse-grained samples the reported range is 5 - 4 GPa for the same range of indentation load [20]. The hardness value asymptotically stabilizes at 4 GPa for loads greater than 100 N. This corresponds to the similar trend observed in the SFF samples. The results obtained conform to the established values for Ti_3SiC_2. An increase in VHN, as we believed, is due to the presence of excessive 30 – 40% of TiC imparting greater hardness to the samples.
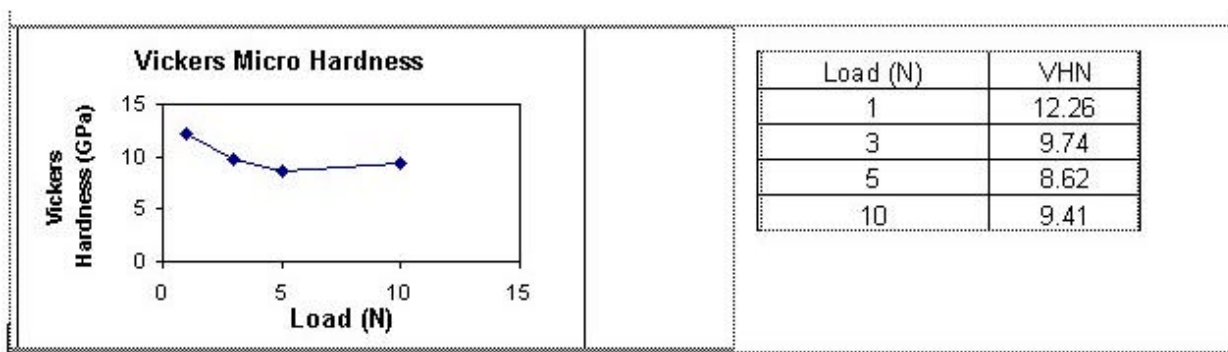

Load (N)	VHN
1	12.26
3	9.74
5	8.62
10	9.41

Figure 7: Vickers Micro Hardness for Ti_3SiC_2 samples

5.3 Damage Tolerance

For the damage tolerance tests the specimens were prepared as per ASTM C1161 type A (25mm x 1.5 mm x 2 mm) along the X and Y directions of SFF Layered Printing. Indentations on these specimens were performed using a Vickers indenter under loads of 100, 200 and 300 N, with one diagonal of the indenter parallel to the length of the specimen. The flexural strength after indentation was determined by a four point bend test as per the procedure in ASTM C 1161 and ASTM C 1211 using a four point flexural fixture. The cross head speed was set for 0.01 mm/s, this corresponds to an average strain rate of 0.0066/s. To remove any surface defects that could act as a crack initiation site under load, the tensile surfaces of the specimens were polished with 1200 grit Silicon Carbide prior to the indentation.

The results for damage tolerance are reported as an average of five measurements taken for each indentation load. The results reported here are for indentation loads of 100, 200 and 300 N. Damage tolerance was recorded as a measure of the breaking strength in a four-point bend test. The retained flexural strength as a result of indentation decreases from 387.33 MPa at no load to 251.67 MPa at 300 N for the sample length along the X-axis of the printing dierction, and decreases from 385 MPa to 242.92 MPa for the sample length along the Y-axis, as shown in Figure 8. The flexural strength of compacted and sintered (without SFF) Ti_3SiC_2 samples has been reported to be in the range of 300 MPa at no load to 240 MPa for a 300 N indentation load in the case of coarse-grained samples [20]. The flexural strength decreased steadily with the increase in the indentation load. This trend is reflected in SFF samples, and the results conform well to the reported data for coarse-grained Ti_3SiC_2.
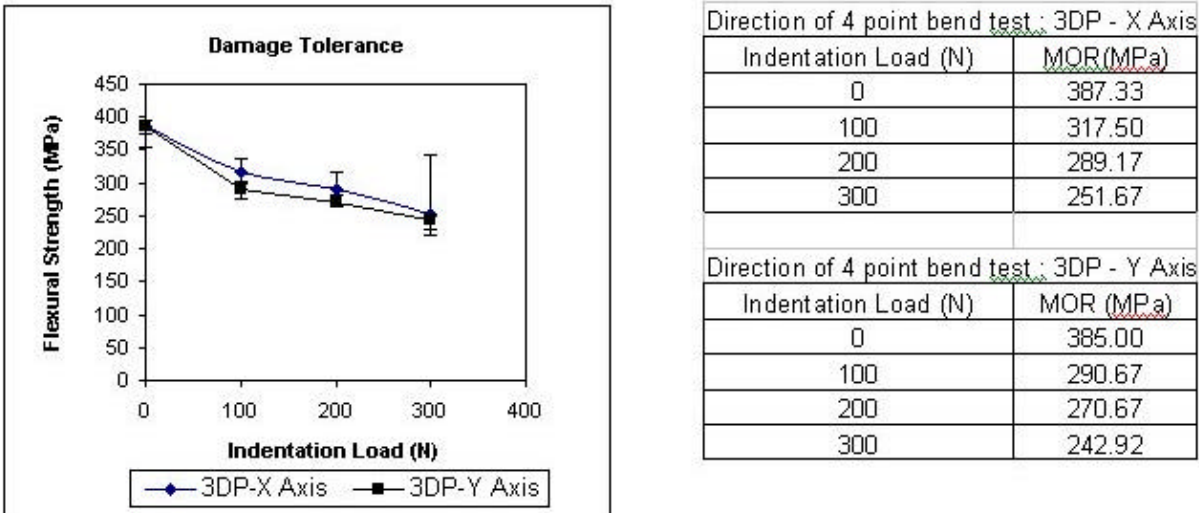

Direction of 4 point bend test : 3DP - X Axis	
Indentation Load (N)	MOR (MPa)
0	387.33
100	317.50
200	289.17
300	251.67

Direction of 4 point bend test : 3DP - Y Axis	
Indentation Load (N)	MOR (MPa)
0	385.00
100	290.67
200	270.67
300	242.92

Figure 8: Damage Tolerance for Ti_3SiC_2 samples

5.4 Thermal Shock

For the thermal shock resistance, specimens conforming to ASTM C1161 type A (25mm x 1.5 mm x 2 mm) along the X and Y directions of the printing were placed in a furnace at the pre-quench temperatures of 400, 800 and 1200 °C, under flowing argon (to prevent the formation of any oxide layers) for 10 minutes. The samples were then immediately quenched into an

ambient temperature water bath. The quenched samples were tested according to the ASTM C1161 and ASTM C 1211 using a four point flexural fixture. All four point bend tests were conducted using a servo-hydraulic MTS Systems testing machine running at a cross head speed of 0.01 mm/s, corresponding to a nominal strain rate of 0.0066 /s. In both cases, thermal shock resistance and damage tolerance, the flexural strength was calculated using the following formula:

$$s = 3\,P\,(l_1 - l_2)\ /\ (2\,B\,W^2)$$

where P is the load at fracture, l_1 and l_2 are the outer and the inner span, respectively, B is the specimen width (2 mm), and W is the specimen thickness (1.5 mm). The four-point bend fixture used had an outer span of 20 mm and inner span of 10 mm. The fixture rollers were free to rotate, but constricted laterally in this setup. The mutual friction between the sample and the rollers was eliminated by the application of a very thin film of anti-friction oil on the roller interface.

The results for thermal shock are reported as an average of five measurements taken for each temperature condition. Thermal shock has been reported as a measure of the flexural strength of the sample under the four-point bend test. The tests were conducted at room temperature, 400 °C, 800 °C and 1200 °C. The retained flexural strengths for the sample length along the X-axis of the printing are in the range of 387.33 – 211.67 MPa and 395 – 174.58 MPa for the sample length along the Y-axis of the printing. The test samples thermally shock up to 400 °C and the Module of Rapture further stabilizes and is retained up to 1200 °C. Beyond 800 °C, an increase in post quench strength is observed in both sample sets, as shown in Figure 9. The flexural strength of compacted and sintered (without SFF) Ti₃SiC₂ samples subjected to thermal shock are about 260 MPa for a temperature of 1400 °C for coarse grained samples and ranging from 560 – 170 MPa over a temperature range of 500 °C to 1100 °C for fine grained samples [20]. It is observed that coarse grained samples retain flexural strength up to a temperature of 1400 °C and are thus thermal shock resistant, whereas fine grained samples thermally shock between 750 °C and 1000 °C [20].
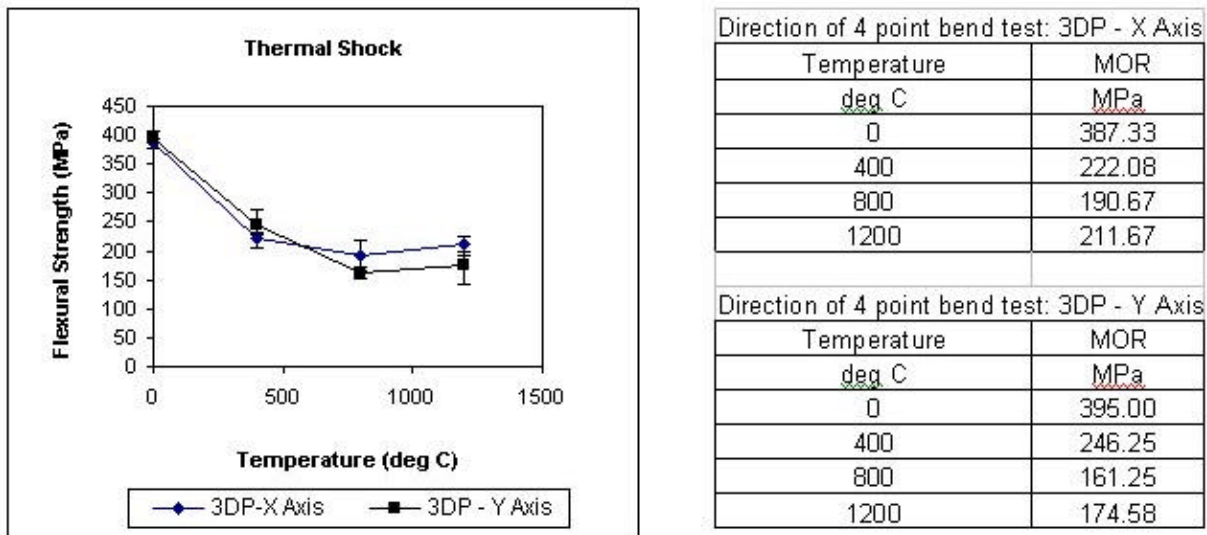

Direction of 4 point bend test: 3DP - X Axis	
Temperature	MOR
deg C	MPa
0	387.33
400	222.08
800	190.67
1200	211.67

Direction of 4 point bend test: 3DP - Y Axis	
Temperature	MOR
deg C	MPa
0	395.00
400	246.25
800	161.25
1200	174.58

Figure 9: Thermal Shock Resistance for Ti₃SiC₂ samples

The test results reflect the reported results of thermal shock resistance and the increasing trend of post quench strength at temperatures of 800 ^{o}C for coarse-grained Ti_3SiC_2. Additionally, it is also observed that the flexural strength along the X-axis of the printing is greater than that along the Y-axis. This is mainly due to the layered nature of the Layered Printing technique. The published results of the Module of Rapture for damage tolerance and thermal shock for Ti_3SiC_2 samples are as per tests conducted without regard for the axis of development. The presented values as per this research demonstrate the anisotropy in strength arrived at as a result of the Layered Printing process.

5.5 Porosity and Shrinkage

The physical shrinkage of each of the samples was measured and calculated as a function of the linear dimensions D, of the individual parts. The shrinkage was calculated as a percentage after each process, namely, Layered Printing, Compacting, and Sintering.

$$\text{Shrinkage} = (D_{\text{pre-process}} - D_{\text{post-process}}) / D_{\text{pre-process}}$$

The percentage porosity is an average of 5 independent representative regions of the sample surface under test. The sample that was derived form the master sample (subjected to the post RP processes of compacting and sintering) had a density of greater than 99%. For the samples developed by varying the binder concentration and layer thickness during the Layered Printing process and directly sintering without compacting, the porosity obtained from the surface calculations of the micrographs show an average porosity of 50 – 60%. This shows that compacting is the dominant process in improving the density of the part. This is quite noticeable comparing the micrographs between Figures 10 and Figure 12. The optical microscope was used to measure the cross-sectional porosities of each sample. The supporting software provides image capture, threshold and density slice tools by which percentage of black and white phases are measured directly. The average porosity for each sample is calculated as a mean value for the data retrieved by the random choice of at least 5 representative points on each sample surface.

The shrinkages after each stage of the integrated process were calculated as a percentage for the sprocket, turbine wheel and tube as listed in Table 1. The average shrinkage measured after the compacting was in the range of 15% and after sintering was about 30%.

Table 1: Shrinkage data for parts developed using the integrated 3-stage process

Sprocket / Turbine:

Geometric Features	Pre-Compact	Post-Compact	Compact	Post Sintering	Compact & Sintering
	inches	inches	% change	inches	% change
Length	1.52	1.33	12.50	1.06	30.07
Width	1.52	1.33	12.50	1.06	30.07
Height	0.50	0.42	16.00	0.36	27.30

Tube:

Geometric Features	Pre-Compact	Post-Compact	Compact	Post Sintering	Compact & Sintering
	inches	inches	% change	inches	% change
Length	1.00	0.81	19.00	0.69	30.70
OD	0.62	0.49	20.97	0.42	31.61
ID	0.30	0.30	0.00	0.22	28.33

5.6 Optical Microscopy

Micrographs of the various samples representing dense and porous structures were acquired using the Olympus PM-3G Optical Microscope. From the micrographs shown in Figures 10, we observe that the part density is in excess of 99% in the planes XY, XZ and YZ through the 3-satge process. The sample structures exhibiting greater than 99% density show a homogeneous distribution of grains without any texture within the powder matrix as shown in Figures 11. The main cause of high density and structural homogeneity is due to the compacting process. In the case of the samples exhibiting porous structure it is observed that the average porosity measured is about 50 - 60% as shown in Figure 12. From the micrographs we observe that the sintering without compacting leads to binder burnout and results in the part being porous. This explains the voids (dark regions) on the micrographs as shown in Figures 12. Further, the increased binder concentration increases the possibility of sintering of a lower quality.

Figure 10: Micrographs of XY, XZ and YZ planes of the master sample
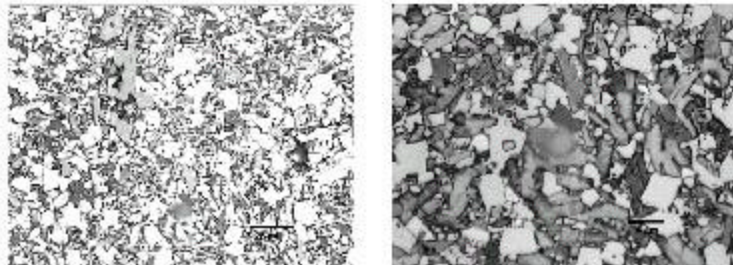With density greater than 99% (200 µm)

Figure 11: Micrographs of the cross-section of the master sample with density
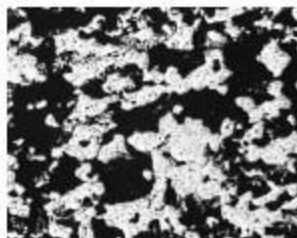greater than 99% at X 500 and X 1000 magnification

Figure 12: Micrograph of sample with porosity at 60% (porous structure) (200 µm)

6. Summary and Conclusions

This paper introduces an integrated process of Layered Printing, Compacting, and Sintering to fabricate highly dense Ti_3SiC_2 structures. Experiments were conducted to study the mechanical characteristics and the effect of the processing parameters on the morphological and structural properties of the fabricated Ti_3SiC_2 structures. The results of the mechanical characterization and the microstructure evaluation of Ti_3SiC_2 structures have been presented. The resulting sintered parts were achieved with a density of greater than 99%. As a post processing surface finishing the parts can be subjected to a grinding and polishing sequence to obtain a mirror finish. As a demonstration of the machinability of the SFF parts, EDM was used to cut the test samples and polished them to obtain required $1\mu m$ surface finish. This integrated process was used to freeform fabricate structures with complex shapes, as shown in Figures 2. A density of greater than 99% was achieved for each of these parts.

The Load – Displacement curves show a linear to failure deformation behavior of the Ti_3SiC_2 specimens. The results of the mechanical characterization for the Ti_3SiC_2 samples also reveal an anisotropy in the mechanical properties, for example, the compressive strength, damage tolerance and thermal shock properties are greater along a certain axis of the printing development. Although the SEM micrographs show a homogeneous grain distribution of Ti_3SiC_2 powder without any texture within the part matrix, we believe that the layered printing process contributes to the anisotropy in the prototyped structure. The results from the tests for compressive strength, hardness, damage tolerance and thermal shock are comparable to the reported data for Ti_3SiC_2, considering the effect of the presence of excessive 30 – 40% TiC in the Ti_3SiC_2 powder used in the fabrication of samples under test.

The samples fabricated using the 3-stage process achieved a density of greater than 99%, while samples without the compacting had a porosity in the range of 50 – 60%. This shows that compacting is the dominant process leading to the high structural density. The average shrinkage measured after compacting was in the range of 15% and after sintering was 30%. The main cause of high density and structural homogeneity is due to the compacting process. A certain amount of warpage was observed after the printing. We believe that this is mainly due to the capillary forces distributed in the powder matrix during the printing process. The maximum warpage occurred along the Y-axis (longest dimension) of the printing and was further enhanced after the compacting process.

In comparison to other Solid Freeform Fabrication methods for prototyping dense and functional structure, the developed 3-stage process is simplicity and cost-effective. However, the process of a larger scale and complicated geometry needs to be developed further to possibly eliminate the compacting process, thus to avoid the part collapse and to retain the designed geometry. The process-induced anisotropy and its relation with the processing parameter and part geometry need also to be further investigated.

References

1.   J. G. Heinrich: "New developments in the solid freeform fabrication of ceramic components", *Ceramic Forum International*, Vol. 76, No. 5, 1999, pp. 29-35.

2. B.K. Paul, S. Baskaran : "Issues in fabricating tooling using powder-based additive freeform fabrication", Journal of Materials Processing Technology 61(1996) pp. 168-172.

3. D. Bourell, H. Marcus, J. Barlow, and J. Beaman, "Selective Laser Sintering of Metals and Ceramics", The International Journal of Powder Metallurgy, Vol. 28, No. 4, 1992, pp. 369-381.

4. E. Sachs, M. Cima, P. Williams, D. Brancazio, and J. Cornie, "Three Dimensional Printing: Rapid Tooling and Prototypes Directly from a CAD Model", Journal of Engineering for Industry, Vol. 114, November 1992, 481-488.

5. J. Moon, J. Grau, P.J. Baker, M. Caradonna, M.J. Cima: "Binder-powder bed interactions in the slurry-based 3-dimensional printing process", *Proceedings of Solid Freeform Fabrication Symposium*, University of Texas, Austin, Texas, 1997.

6. J. Grau, J. Moon, M.J. Cima: "Structural ceramics fabricated by 3-dimensional printing", *Proceedings of Solid Freeform Fabrication Symposium*, University of Texas, Austin Texas, 1997.

7. S. Rock and C. Gilman, "A New SFF Process for Functional Part Rapid Prototyping and Manufacturing: Freeform Powder Molding," *Proceedings of Solid Freeform Fabrication Symposium*, University of Texas, Austin, Texas, 1995.

8. M. Agarwala, et al, "Structural Ceramics by Fused Deposition of Ceramics", *Proceedings of Solid Freeform Fabrication Symposium*, University of Texas, Austin, TX, 1995.

9. S. Uhland, R. Holman, B. DeBear, P. Saxton, M. Cima, E. Sachs, Y. Enokido and H. Tsuchiya: "Three-dimensional printing, 3DP^{TM}, of electronic ceramic components", *Proceedings of Solid Freeform Fabrication Symposium*, University of Texas, Austin, TX, 1999, pp. 865-872.

10. M. Greul, T. Pintat, M. Greulich : "Rapid Prototyping of Functional Parts", Advances in Powder Metallurgy and Particulate Materials. 3, 1997. Metal Powder Industries Federation, Princeton, NJ, USA. p 18-153-159.

11. P.B. Blazdell, J.R.G. Evans: "Application of continuous ink jet printer to solid freeforming of ceramics", *Journal of Materials Processing Technology*, Vol. 99, 2000, pp. 94-102.

12. M. Mott, J.-H. Song and J. Evans: "Microengineering of ceramics by direct ink-jet printing", *Journal of American Ceramics Society*, Vol. 82, No. 7, 1999, pp. 1653-58.

13. J.Cesarano, "Robocasting: Direct fabrication of ceramics from colloidal suspensions", *Proceedings of Solid Freeform Fabrication Symposium*, University of Texas, Austin, TX, 1997.

14. J. Windle, B. Derby: "Ink jet printing of PZT aqueous ceramic suspensions", *Journal of Materials Science Letters*, Vol. 18, 1999, pp. 87-90.

15. A.V. Kumar and H. Zhang: "Electro photographic powder deposition for freeform fabrication", *Proceedings of the 11th Solid Freeform Fabrication Symposium*, University of Texas, Austin, 1999, pp. 647-653.

16. M.J. Wright, R.G. Evans: "Ceramic deposition using an electromagnetic jet printer station", *Journal of Materials Science Letters*, Vol. 18, 1999, pp. 99-101.

17. D. J. DCosta. S. D. Dimovski, F. Lin, T. El-Raghy, M. W. Barsoum and W. Sun: "Three Dimensional Printing of Layered, Machinable, Ductile Carbide", *Proceedings of the 11th Solid Freeform Fabrication Symposium*, University of Texas, Austin, August 2000.

18. T. El-Raghy and M. W. Barsoum: "Synthesis and Characterization of a Remarkable Ceramic: Ti$_3$SiC$_2$", *Journal of American Ceramics Society*, Vol. 79, No. 7, 1999, pp. 1653-58.

19. T. El-Raghy and M W. Barsoum: "Processing and mechanical properties of Ti$_3$SiC$_2$, Part I: Reaction Path and Microstructure Evolution", *Journal of American Ceramics Society*, Vol. 82, 1996., pp. 1953-56.

20. T. El-Raghy, M. W. Barsoum, A. Zavaliangos and S. R. Kalidindi: "Processing and mechanical properties of Ti$_3$SiC$_2$, Part II: Mechanical properties", *Journal of American Ceramics Society*, Vol. 82, 1999., pp. 2855-60.

21. W. Sun, D. J. Dcosta, and T. El-Raghy, "Fabrication of Three-dimensional Fully Dense Ti$_3$SiC$_2$ Structures," US Patent, (pending).